



Fabrication of a ternary plasmonic photocatalyst CQDs/Ag/Ag₂O to harness charge flow for photocatalytic elimination of pollutants

Jibin Chen, Huinan Che, Kai Huang, Chunbo Liu*, Weidong Shi*

School of Chemistry and Chemical Engineering, Jiangsu University, Zhenjiang 212013, PR China

ARTICLE INFO

Article history:

Received 29 January 2016

Received in revised form 18 March 2016

Accepted 24 March 2016

Available online 25 March 2016

Keywords:

CQDs/Ag/Ag₂O

Photocatalytic activity

Operational stability

Full-spectrum

Vectorial charge-transfer

ABSTRACT

The photocatalytic technology provides a straightforward and effective strategy for the ever-increasing environmental and energy concerns. In this study, a practical strategy is proposed to facilitate the separation of e-h pairs and enhance the photostability in a semiconductor by the use of a Schottky junction in a noble metal-CQDs-semiconductor stack structure (CQDs, carbon quantum dots). Different characterization techniques were used to investigate the structural and optical properties of the synthesized samples. Importantly, due to the photoinduced electron transfer and upconversion luminescence properties of CQDs, the CQDs/Ag/Ag₂O ternary photocatalysts exhibit excellent photocatalytic activity and operational stability in full-spectrum. Furthermore, Ag nanoparticles supported on an ultrathin CQDs layer encapsulating Ag₂O octahedral crystal lead to the highest photocatalytic activity by the synergetic catalytic effect of interfacial modification and vectorial charge-transfer channel design. Our works provide an invaluable methodology for the development of practical photocatalysts in current environmental pollution, energy issues and other related areas.

© 2016 Elsevier B.V. All rights reserved.

1. Introduction

The exploration and configuring of new photocatalytic materials with good stability and high catalytic efficiency have been considered to be one of the important investigative fields for the solar energy conversion and the destruction of organic pollutant [1]. Up to now, numerous semiconductor photocatalysts have been researched, such as TiO₂ [2,3], Cu₂O [4], SrTiO₃ [5]. However, the potential application of photocatalyst is still limited for the rapid recombination rate of electron-hole pairs, poor stability and the low utilization of solar energy [6]. Therefore, the development of novel photocatalysts to improve both the photochemical activity and stability is urgent and indispensable. To achieve these objectives, an ideal photocatalytic system should at least have the following these characteristics: efficient electron-holes pair separation capacity, effectively activated by near infrared (NIR) and IR light (collectively called (N)IR) and operational stability.

Among the various semiconductors, silver oxide (Ag₂O), as a direct semiconductor with a narrow band gap of 1.19 eV, and the search for Ag₂O has been widely used in many industrial fields, such as a catalysts for alkane activation and epoxidation and as

an electronic device in Zn-Ag₂O battery [7]. Given these favorable attributes, Ag₂O have received much attention in environmental remediation for its high absorption of visible light. Nevertheless, the practical photochemical application of Ag₂O are seldom for the poor capability to separate electron-hole pairs and the self-photocorrosion property. Therefore, it's a challenge to attempt to ameliorate both the photochemical activity and stability of Ag₂O for the practical application, especially for the harvesting of all solar light.

It is well-known that construct specific stack architectures can solve above problem to a certain extent. Up to now, many stack architectures have been successfully prepared for a favorable electron pathway, such as Cu₂O → graphene → Au-Cu nanoalloys [4], CdS → Au → SrTiO₃ [5], CdS → Au → TiO₂ [8] and AgVO₃ → RGO → Ag [9]. Therefore, it is necessary to explore the method of constructing the stack architectures photocatalyst to achieve the maximum degree of the electron hole pair separation, and promote the harvest the full spectrum. Recently, plasmonic photocatalyst were designed to broaden optical applications and ameliorate the catalytic ability [10–13]. Several metal deposited photocatalysts have been reported, such as Ag@AgCl [14], Bi/BiOCl [15] and Cu/graphene/Cu₂O [4]. These metal surface plasmon resonance (SPR) cannot only absorb more solar light, but also enhancing the surface electron excitation and interfacial electron transfer. As one of the most impressive plasmonic metals, Ag has always

* Corresponding author.

E-mail addresses: liuchunbojsu@163.com (C. Liu), swd1978@uj.edu.cn (W. Shi).

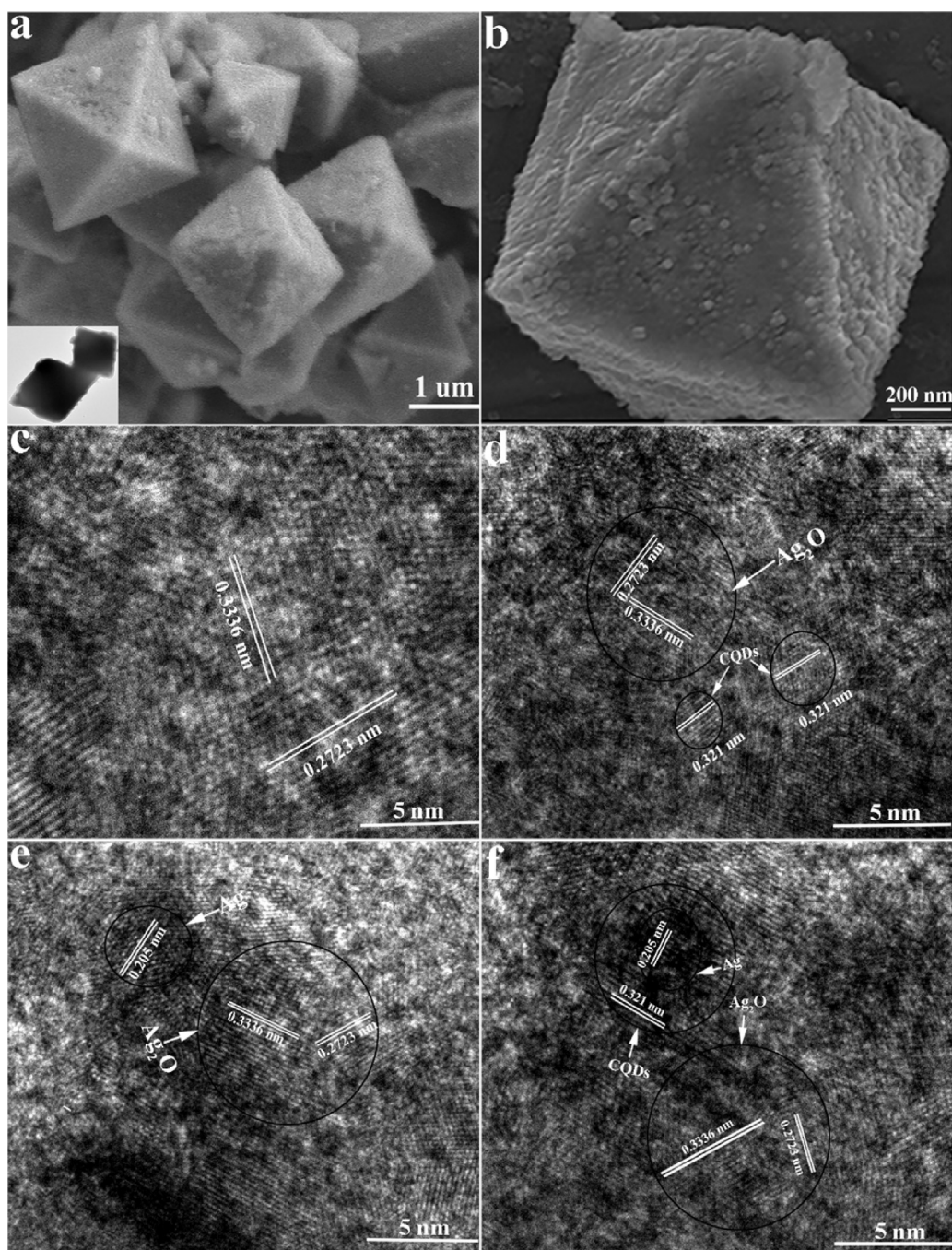
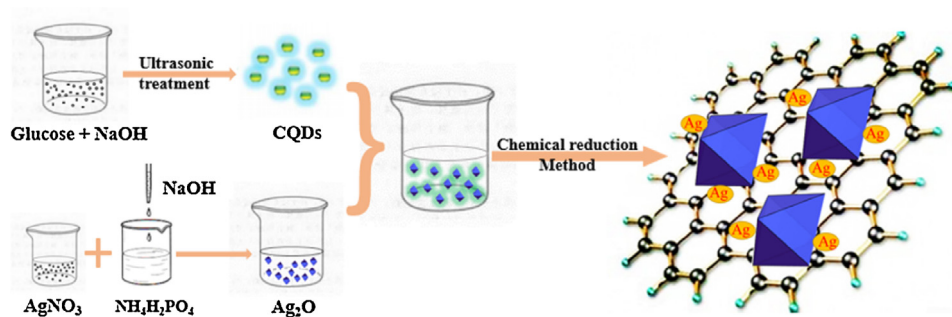
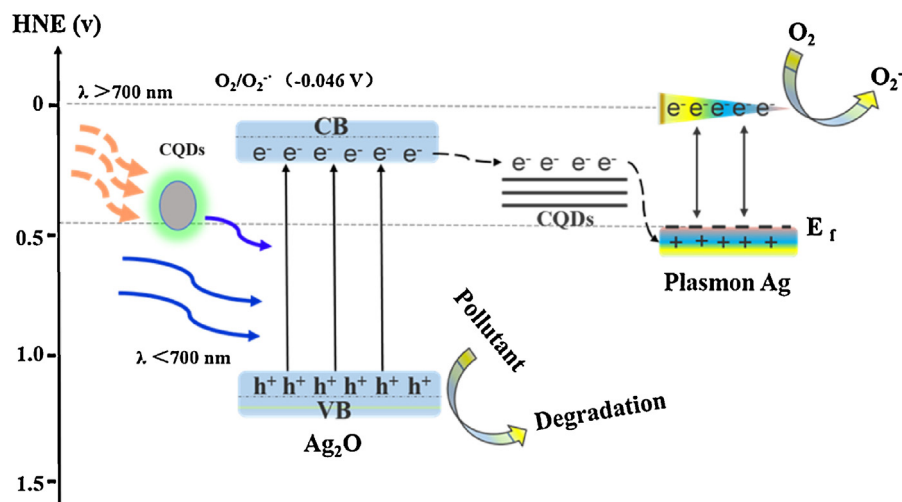


Fig. 1. (a) SEM and (b) FESEM image of CQDs/Ag/Ag₂O ternary photocatalyst. HRTEM image of Ag₂O composites: (c) pure Ag₂O, (d) CQDs/Ag₂O, (e) Ag/Ag₂O, (f) CQDs/Ag/Ag₂O, respectively.



Scheme 1. Synthesis Process of the CQDs/Ag/Ag₂O Nanocomposites.



Scheme 2. A proposed reaction mechanism for full spectrum degradation organic pollution on CQDs/Ag/Ag₂O nanocomposites.

provide more active sites upon which the associated chemical transformations have occurred on the surface of the corresponding semiconductor with lower activation barriers [16–19]. This has given us beneficial enlightenment: similarly, the photocatalytic activity of Ag₂O would be improved if the Ag grafted on the surface of the sample, in which the vectorial electron transfer is favored by forming electronic coupling based on the cascade energy alignments and the built-in electric field in metal/semiconductor junctions [20,21]. However, on the basis of the high catalytic activity, it is still a great challenge to ensure that it can be recycled. Carbon material is known to have excellent electrical conductivity, nontoxicity and feasibility form the insoluble carbon layer on the surface of semiconductor, which can greatly improve the structural stability during the photocatalytic process [22,23]. For example, TiO₂/RGO/Cu [24], C/Cu₂O [22] and CQDs/Ag₃PO₄ [25] composite successfully revealed that the thin carbon-layer-protected semiconductor not only exhibited remarkably improved photostability but also showed significantly ameliorated catalytic activity. In addition, CQDs have been commonly used as photosensitizers for their display abundant unique photo-physical and chemical properties [26–29]. Especially, the photoinduced electron-transfer and excitation wavelength dependent photoluminescence (PL) behaviors, which make CQDs-based (N)IR light sensitive hybrid photocatalysts become promising agents for harvesting (N)IR light [30,31]. Considering such remarkable properties, we proposed a novel metal-CQDs-semiconductor stack design offers as specific nanostructured architectures, which will attempt to balance charge separation, responding spectrum area and stability.

In this work, we report a general method for the fabrication of CQDs/Ag/Ag₂O ternary plasmonic photocatalyst in which ultrathin CQDs insoluble layers encapsulating Ag₂O octahedral structure supporting the optimized combination of Ag nanoparticles are used as the synergetic catalysts. The as-synthesized CQDs/Ag/Ag₂O ternary plasmonic photocatalyst displays the most excellent charge separation ability and highest catalytic performance among all the catalyst system. Meanwhile, the key roles of Ag particles and CQDs layers in complex photocatalysts were thoroughly investigated, respectively. Moreover, due to the fluorescence effect of CQDs, it is also have excellent electrical conductivity, and the synergy of its have laid a solid foundation for the photocatalytic performance of the whole system.

2. Experimental

2.1. Synthesis of CQDs

CQDs were prepared through a simple one-step alkali-assisted ultrasonic methods. In a typical procedure, a suitable amount of glucose was dissolution in deionized water to form a colorless solution (1 mol/l). Certain concentrations NaOH solution was added to the solution of glucose under magic stirred, then the mixed solution was subjected to an ultrasonic treatment for 3 h. Then, the crude sample (20 ml) obtained from glucose/NaOH was adjusted to pH = 7 with HCl. After that, the crude solution was further dialyzed in a dialysis bag (MWCO 1000) overnight and CQDs with strongly flurescent were obtained through the dialysis bag. After dialyzed treatment, the obtained solution was brown, implying the formation of CQDs.

2.2. Synthesis of CQDs/Ag₂O and Ag₂O

0.153 g AgNO₃ and 0.230 g NH₄H₂PO₄ were well dissolved in 100 ml CQDs aqueous solution. NaOH aqueous solution (2 M) was added drop by drop to the above solution, until the pH value of the mixed solution was adjusted to 11, then the resulting mixture was subjected to be constant magnetic stirring at room temperature for 12 h in the dark. The obtained CQDs/Ag₂O samples were washed, centrifuged several times with deionized water and ethanol, and finally dried at 60 °C for 6 h. Finally, the CQDs/Ag₂O sample were obtained. The Ag₂O catalysts were simply prepared in the process of synthesis of water instead of CQDs solution.

2.3. Synthesis of Ag/Ag₂O and CQDs/Ag/Ag₂O

The CQDs/Ag/Ag₂O complex photocatalysts were synthesized by the homogeneous precipitation method. Typically, 0.155 g AgNO₃ were dissolved in 100 ml CQDs aqueous solution. Subsequently, 2 drops NaBH₄ aqueous (1 M) was added drop by drop to the above solution and stirred for 1 h. During the reaction, Ag⁺ in solution can be easily reduced into Ag and attached onto the surface of catalyst. Subsequently, excess 5 M NaOH aqueous was added drop by drop until the pH reached 11. After reaction for 3 h, the obtained CQDs/Ag/Ag₂O samples were washed with water to remove the NO₃⁺ and excess OH⁻, and finally dried at 60 °C for 6 h. The process is shown in Scheme 1. For comparison, the Ag/Ag₂O

catalysts were simply prepared by replacing the CQDs aqueous solution with water.

2.4. Materials characterization

All of the phase compositions and crystal structures of the prepared samples were determined by powder X-ray diffraction (XRD) method using Cu K α radiation ($\lambda = 1.54178 \text{ \AA}$). An S-4800 field emission scanning electron microscope (FESEM) was used to observe the morphology of as-prepared samples. The transmission electron microscopy (TEM) and high-resolution TEM (HRTEM) were also used to characterize the sample by transmission electron microscopy (Tenai G2 F30 S-Twin, FEI) using an accelerating voltage of 200 KV. The Fourier Transform Infrared (FT-IR) spectrum was recorded on a Bruker Vertex 70 spectrometer using KBr as the dispersion medium. The ionic characteristics were obtained by X-ray photoelectron spectroscopy (XPS) on a Thermo ESCALAB 250X (America) electron spectrometer. UV-vis-NIR diffuse reflectance spectra (DRS) were obtained by a UV-vis-NIR spectrophotometer (Cary 5000, Varian). The PL spectra were carried out on a Horiba JobinYvon (FluoroMax 4) Luminescence Spectrometer. Electrochemical impedance spectroscopy (EIS) was performed in the frequency range of 10^5 – 10^{-2} Hz with the initial potential (0V) in 0.5 M H $_2$ SO $_4$. Time-resolved photoluminescence spectroscopy (TRPS) spectra were obtained on a Model FES 920 system with an excitation wavelength of 337 nm and detection wavelength of 469 nm.

2.5. Photocatalytic experiments

The photodegradation experiment of a methylene blue (MB) and rhodamine B (RhB) solution (10 mg l^{-1}) was carried out under UV, visible and (N)IR light irradiation. In a typical photocatalytic experiment, 50 mg of as-synthesized samples was dispersed with vigorous stirring in 100 ml pollutants aqueous solution (10 mg/l) and ensure to establish adsorption-desorption equilibrium. A 250 W xenon lamp was used as the visible light source with filter glasses ($<420 \text{ nm}$) and without the filter glasses as the simulated sunlight. A 150 W infrared lamp used as the (N)IR light source where the $\lambda < 700 \text{ nm}$ light were completely removed. At given irradiation time intervals, the residual pollution concentration was detected after centrifuged (10,000 rpm, 10 min) by the UV-vis spectrophotometer at a specific wavelength. In addition, thermal decomposition controlled trials of as-prepared sample was further estimated by the decomposition of MB and RhB under isothermal conditions.

3. Results and discussion

3.1. Characterization of as-prepared photocatalysts

The preparation of CQDs from glucose could be achieved by the simple ultrasonic synthetic method, the TEM images, Raman spectrum, FT-IR spectrum and UV-vis absorption spectrum of the CQDs were displayed in Fig. S1, which are similar to the CQDs structure publicly reported [25,30]. The morphology and structures of the as-synthesized different samples were characterized by FESEM and TEM. The TEM (inset in Fig. 1a) and SEM shows the overall views of the Ag $_2$ O nanoparticles, which revealing the octahedral structure with average diameter of ca. 800–1000 nm. The SEM image of a single CQDs/Ag/Ag $_2$ O particle (Fig. 1b) demonstrate no obvious difference of size and morphology between pure Ag $_2$ O and CQDs/Ag/Ag $_2$ O composite. Fig. 1c shows a HRTEM image of pure Ag $_2$ O. It can be seen that the Ag $_2$ O have two interplanar spacings of 0.3336 and 0.2723 nm, which corresponds to the (110) and

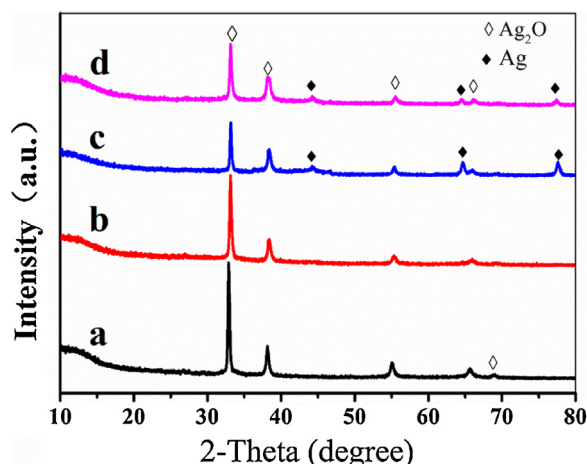


Fig. 2. XRD patterns of (a) Ag $_2$ O, (b) CQDs/Ag $_2$ O, (c) Ag/Ag $_2$ O, (d) CQDs/Ag/Ag $_2$ O.

(111) lattice planes, respectively. As shown in Fig. 1d, after assembling CQDs on the surface of Ag $_2$ O, in addition to the previously described Ag $_2$ O lattice, the lattice spacing of 0.321 nm agrees well with the (002) spacing of graphite was observed [26]. It can be seen from Fig. 1e that the lattice spacing of Ag particles is measured to be 0.205 nm, which according to the (200) crystal plane [14]. Fig. 1f shows the HRTEM image of CQDs/Ag/Ag $_2$ O sample, demonstrating a similar octahedral morphology to that of CQDs/Ag $_2$ O. Besides the Ag $_2$ O lattice spacing, the HRTEM image in Fig. 1f also displays CQDs and Ag lattice spacing simultaneously. Based on the above-mentioned results of SEM/TEM images, the formation of the plasmonic Ag supported on the composite photocatalysts of ultrathin CQDs shell encapsulating Ag $_2$ O is confirmed. Fig. S2 shows the energy dispersive spectroscopy (EDS) patterns of Ag $_2$ O and the related complex material. The spectroscopy in Fig. S2a and b displays peaks of O and Ag elements except for the C from the carbon substrate, respectively. For the EDS of Fig. S2c and d, we can see that the C peak can be clearly increased, which attribute to the CQDs of introduce in the complex photocatalysts.

The different sample was characterized by XRD, and the sharp peaks (Fig. 2) indicated Ag $_2$ O crystal domains with the octahedral structure (JCPDS no. 41-1104). The XRD patterns of prepared Ag/Ag $_2$ O sample indicate that the samples are well crystallized and the crystal phase of Ag $_2$ O does not change with forming Ag nanoparticles on the Ag $_2$ O surface. However, no signal that is attributable to the CQDs can be observed in the CQDs/Ag $_2$ O or CQDs/Ag/Ag $_2$ O composites, which may due to the low CQDs content. The result can also be observed in similar system [25,31]. For the CQDs/Ag/Ag $_2$ O composite, the obvious and sharp features of the observed Ag and Ag $_2$ O characteristic peaks suggest the co-existence of distinguishable models.

High-resolution XPS was performed to analyze the surface chemical compositions and the bonding characteristics of as-prepared pure Ag $_2$ O and CQDs/Ag/Ag $_2$ O. Fig. 3a represents the typical full survey XPS spectrum of as-prepared sample, which further suggesting the as-synthesized sample is composed of silver, oxygen and carbon elements without impurities. For the Ag $_2$ O sample, the spin-orbit components of Ag 3d peak are centered at approximate 374.2 and 368.4 eV, which corresponding to Ag $^+$ in crystal structure (Fig. S3). Interesting, from XPS spectra of the Ag species of the CQDs/Ag/Ag $_2$ O composite (Fig. 3b), the two strong peaks can be further decomposed into four bands (368.3, 369.5, 374.6, and 375.7 eV), implying the presence of different valence of silver species. The two relatively weak peaks at 369.5 and 375.7 eV are attributed to Ag 0 3d $_{5/2}$ and 3d $_{3/2}$, respectively. This result coincides with published reports [9]. The high-resolution O 1s spec-

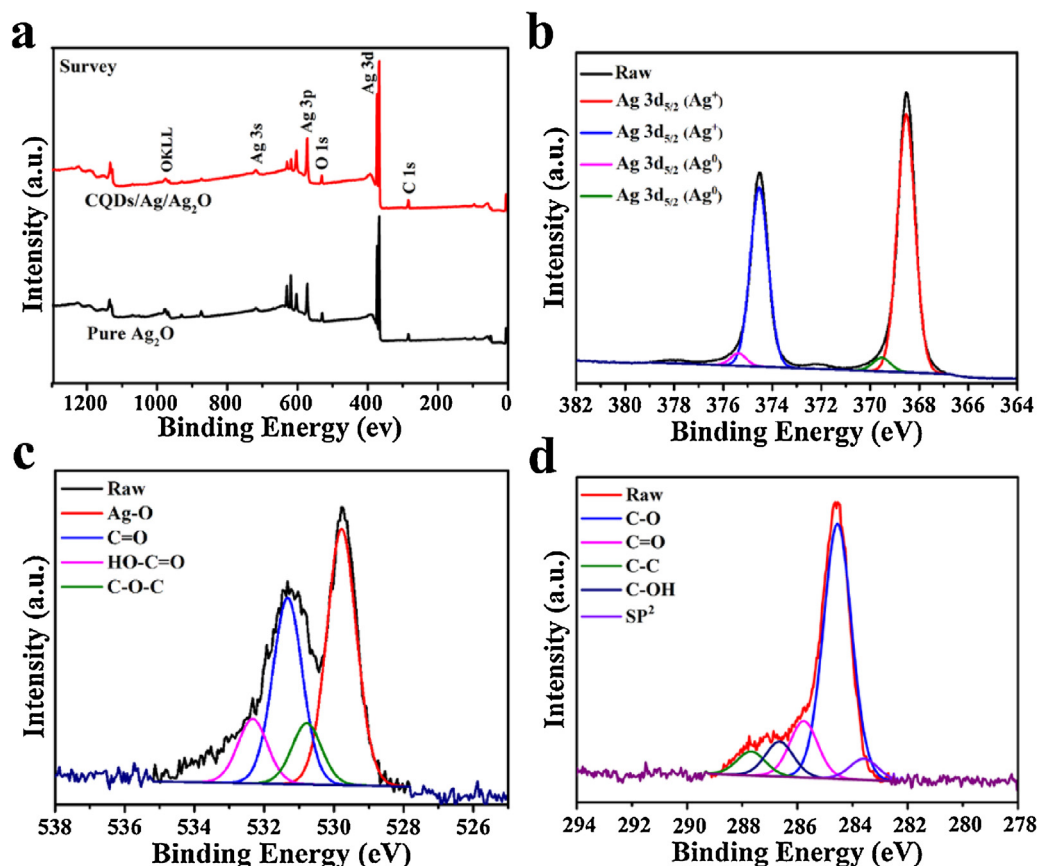


Fig. 3. XPS spectra of the pure Ag_2O and CQDs/Ag/ Ag_2O hybrid. (a) Survey of the sample; (b) Ag 4f; (c) O 1s and (d) C 1s.

trum may be ascribed to the O elements in CQDs/Ag/ Ag_2O crystals is shown in Fig. 3c. A broad and strong peak could be divided into four peaks. An Ag-O characteristic peak appeared at 529.4 eV, while the other high resolution O 1s peaks respectively centered at 531.8 eV, 532.9 eV and 534.3 eV, which assigned to C=O, HO-C=O and C-O-C peaks. Fig. 3d displayed the XPS spectrum of the C 1s, which revealed the surface function groups on the CQDs. As shown, the five peaks are respectively located at 283.7, 284.6, 285.8, 286.7 and 287.8 eV, which attributed to C-O, C=O, C-C, C-OH and SP^2 hybridization of carbon, respectively [33,34]. Significantly, the Ag 3d and O 1s peaks positions in the CQDs/Ag/ Ag_2O sample show a slight shift when compared to the Ag 3d and O 1s peaks in the Ag_2O sample (Fig. S3b and c). This indicates that the chemical environment of CQDs and Ag in ternary photocatalyst has changed and can be deduce the presence of C-Ag interaction. The results reveal that the CQDs and Ag composites can efficiently combine with the Ag_2O substrate to form bonding, which is the key to enhance the electronic separation and improve the photocatalytic activity.

The possible interactions among CQDs/Ag/ Ag_2O nanoparticles was further confirmed by Raman and FT-IR spectra. As shown in Fig. 4a, the FT-IR was used to analyze the change in functional groups during the synthesis process. In the FT-IR analysis of CQDs, abundant hydroxyl groups on the CQDs surface can be identified from the FT-IR spectrum of pure CQDs, e.g., 3430 cm^{-1} for stretching vibrations of C-OH and 2923 cm^{-1} for C-H, 1126 cm^{-1} for asymmetric stretching vibrations of C-NH-C, 1570 cm^{-1} for bending vibrations of N-H, and 1635 cm^{-1} for the vibrational absorption band of C=O [35,36]. For CQDs/ Ag_2O and CQDs/Ag/ Ag_2O , the characteristic peaks of C-OH, C-H and N-H were observed at same wavelength, which indicating the existence of CQDs in the complex photocatalysts. While the Raman was obtained, as shown Fig. 4b, two typical Raman bands located at about 1335 and 1610 cm^{-1} for

the studied samples registered, which are associated with disordered sp^3 carbon (D-band) and conjugated sp^2 (G-band) of carbon atoms, respectively [37,38]. Significantly, it is manifest that the CQDs/Ag/ Ag_2O shows a higher intensity as compared with that of CQDs/ Ag_2O , which can be attributed to the surface-enhanced Raman scattering activity of Ag nanoparticles [9]. In addition, a down-shift of D-band and G-band were observed for CQDs/Ag/ Ag_2O and CQDs/ Ag_2O compared with CQDs, which provides further evidence for chemical bonding of carbon materials [39]. Based on the above evidence, we can conclude that Ag particles and CQDs are chemically bonded to the Ag_2O surface. These chemical bonds are vital importance to the catalytic activity and stability of the composite.

In order to obtain an excellent photocatalyst, the study of the relationship between light and photocatalyst is essential. Fig. 4c shows the optical absorption spectroscopy of Ag_2O , Ag/ Ag_2O , CQDs/ Ag_2O and CQDs/Ag/ Ag_2O samples. It can be seen that pure Ag_2O can absorb visible light with 700 nm wavelength were in good agreement with the band gap of 1.9 eV , while Ag/ Ag_2O shows an intense and broad background absorption due to surface plasmon resonance. Interesting, both CQDs/ Ag_2O and CQDs/Ag/ Ag_2O exhibit continuous strong absorption in the range of $250\text{--}2500\text{ nm}$, which implies that these two complex photocatalysts may result in higher photocatalytic activity by excited to produce more electron-hole pairs under the same light irradiation. Fig. 4d shows the DRS reflectance spectrum comparison between different composite samples and pure Ag_2O . It can be seen that the pure Ag_2O indeed has higher light reflectance than others compound in the range of the light is $700\text{--}2500\text{ nm}$, further demonstrating the composite has a better light absorption capacity, especially after loading the CQDs. These experimental phenomenon again proving that CQDs may be used as a powerful energy-transfer component in the design

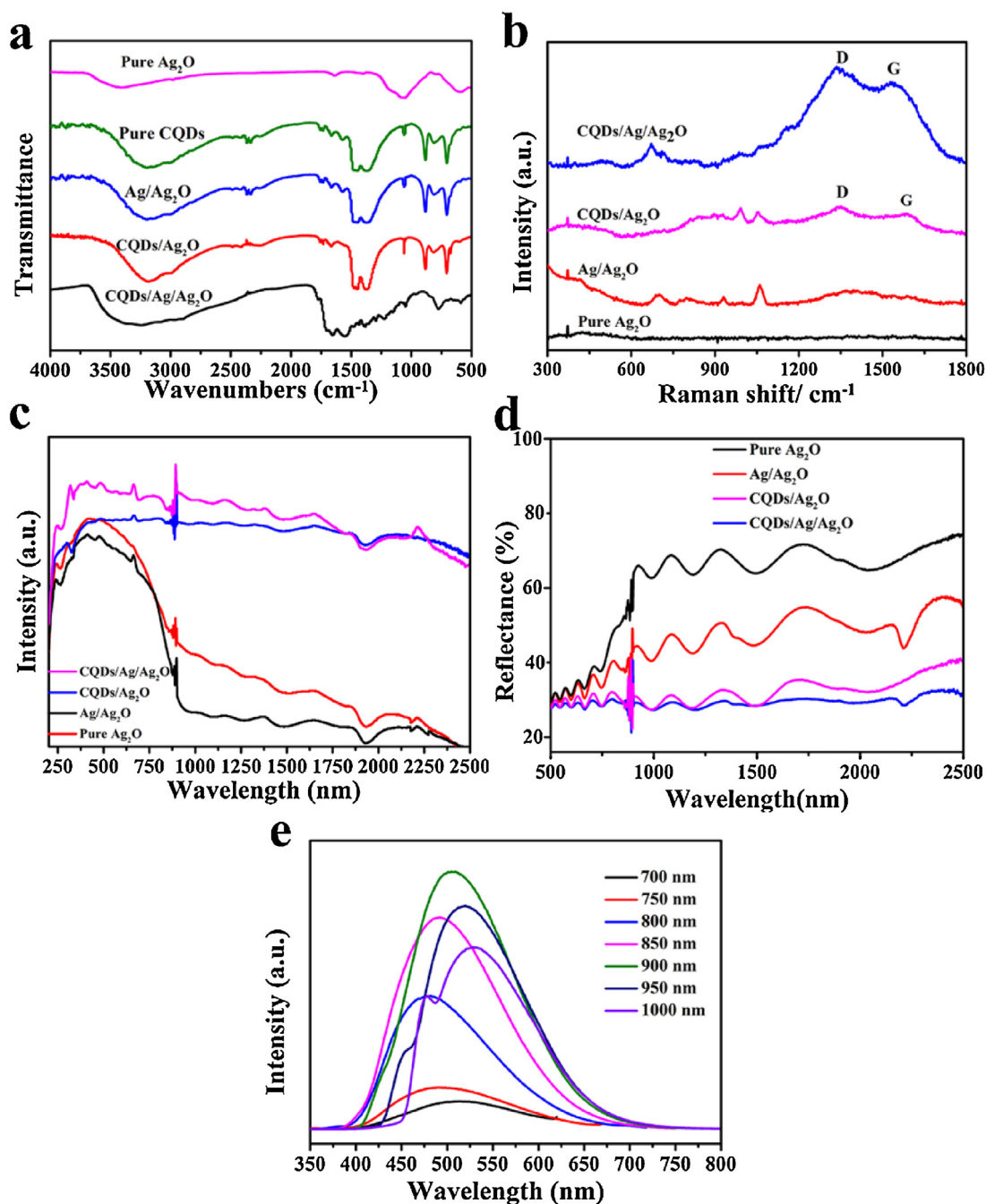


Fig. 4. (a) FT-IR spectra; (b) Raman spectra; (c) Optical absorption spectroscopy; (d) UV-vis-NIR DRS reflectance spectra of for pure Ag_2O , $\text{Ag}/\text{Ag}_2\text{O}$, $\text{CQDs}/\text{Ag}_2\text{O}$ and $\text{CQDs}/\text{Ag}/\text{Ag}_2\text{O}$; (e) up-converted photoluminescence spectra of CQDs.

of new catalyst design towards environmental issues. In addition, the upconverted photoluminescence spectra of CQDs under different excitation wavelength was obtained (Fig. 4e). We found that CQDs can absorb (N)IR light and then emit photoluminescence at a shorter wavelength as a result of up-conversion. That is to say, the broad spectrum of sunshine can be used to excite Ag_2O through up-conversion process.

A series of experiments was measured to verify the $\text{CQDs}/\text{Ag}/\text{Ag}_2\text{O}$ ternary system could the charge-carrier migration behavior and inhibit the recombination of charge-pairs. As shown in Fig. 5, the Nyquist curve of the EIS indicate that the charge transfer resistance of the system is significantly reduced by the usage of Ag and CQDs layer, given that the semicircle in a Nyquist curve are often employed to characterize the charge-transfer process while

the diameter of the semicircle represented the internal resistance of electrode-electrolyte in the electrolyte [40,41]. Note that the arc radius of the Nyquist curve for $\text{Ag}/\text{Ag}_2\text{O}$ and $\text{CQDs}/\text{Ag}_2\text{O}$ is smaller than that of pure Ag_2O , which indicated that both of them has a resistance lower than that of pure Ag_2O . Furthermore, the prominently decreased in the impedance was obtained for the $\text{CQDs}/\text{Ag}/\text{Ag}_2\text{O}$ is compared to that of before. This result showed that CQDs may serve as electron transfer media in the vectorial electron transfer of $\text{Ag}_2\text{O} \rightarrow \text{CQDs} \rightarrow \text{Ag}$, thus promoted interfacial charge separation and migration, efficiently reduce excitation quenching and energy dissipation.

To further demonstrate the importance of the dynamic electron migration process, as shown in Fig. 6, we also measured the time-resolved photoluminescence spectra. Obviously, the four curves

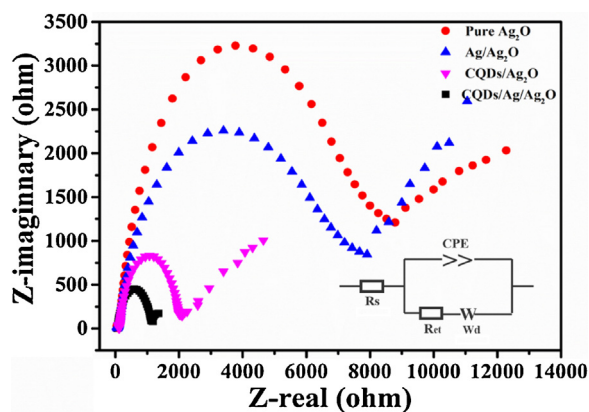


Fig. 5. Nyquist plots for pure Ag_2O , $\text{Ag}/\text{Ag}_2\text{O}$, $\text{CQDs}/\text{Ag}_2\text{O}$, and $\text{CQDs}/\text{Ag}/\text{Ag}_2\text{O}$.

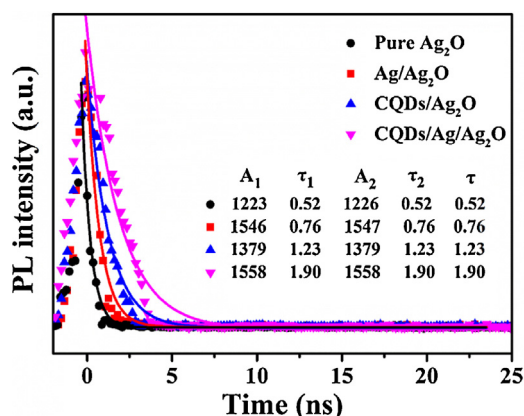


Fig. 6. Time-resolved fluorescence decay curves of pure Ag_2O , $\text{Ag}/\text{Ag}_2\text{O}$, $\text{CQDs}/\text{Ag}_2\text{O}$ and $\text{CQDs}/\text{Ag}/\text{Ag}_2\text{O}$, respectively. Excitation and detection wavelengths are 337 and 469 nm, respectively.

exhibits a fast decay feature in nanosecond scale, which indicates that the charge recombination rate of Ag_2O is bound to receive a certain constraint [42,43]. After fitting the curves with exponential model, the lifetime of as-prepared pure Ag_2O , $\text{Ag}/\text{Ag}_2\text{O}$, $\text{CQDs}/\text{Ag}_2\text{O}$ and $\text{CQDs}/\text{Ag}/\text{Ag}_2\text{O}$ samples were 0.52, 0.76, 1.23 and 1.90 ns, respectively. That is, 0.52 ns is the intrinsic fluorescence lifetime of the Ag_2O , which is related to the recombination of the electron-hole pairs under the excitation of light. Compare with the pure Ag_2O , the lifetime was significantly prolonged when CQDs and Ag were introduced simultaneously. The prolonged lifetime of charge carriers indicating an accelerated charge transfer mechanism induced by the loading of the CQDs and Ag nanoparticles. Interesting, the $\text{CQDs}/\text{Ag}/\text{Ag}_2\text{O}$ array induced the longest decay time indicates have a fast electron transfer via $\text{Ag}_2\text{O} \rightarrow \text{CQDs}$ layer $\rightarrow \text{Ag}$ particles. The accelerated charge transfer is bound to enhance the photocurrent and photocatalytic activity. These results also demonstrate that Ag nanoparticles can effectively store the photogenerated electrons in the photocatalytic system.

3.2. Photocatalytic performance

As we all know, as major influencing factor, the loading amount of Ag or CQDs in complex system should also be noted. Fig. 7 displays the effects of Ag particles loading amount and CQDs adsorbed amount on the photoactivity for degradation performance over pure Ag_2O . As shown in the diagram, the photocatalytic activity was improved with the increasing of loading amount of Ag particles or CQDs. When the loading amount of Ag and CQDs respectively reach to 0.40 wt% and 30 ml, the degradation activ-

ity was the best. However, the degradation rate of MB gradually decreased when the loading amount of silver and CQDs exceeded the fixed value. This phenomenon should be reasonably attributed to the fact that surplus Ag or CQDs can hinder the production of active radicals by block the electron/hole pairs reacting with the adsorbed oxidants/reducers (usually O_2/OH^-). On the other hand, this phenomenon may also be due to the competitive between light harvesting and active sites of photocatalytic degradation.

Based on above experimental condition, we select the best loading amount of sample to carry out the photocatalytic activity for the degradation of MB and Rh B under UV, visible and (N)IR light irradiation (Fig. 8a–c). The photocatalyst (50 mg) was added into the contaminant solution (100 ml). Prior to irradiation, the suspension was magnetically stirred to ensure achieved the adsorption-desorption equilibrium after dark reaction for 60 min. The blank trial reveals that the photolysis of MB or Rh B molecule was very slow and negligible. As shown in Fig. 8a, the photodegradation efficiency of MB over $\text{CQDs}/\text{Ag}/\text{Ag}_2\text{O}$ ternary plasmonic photocatalyst is more than 95% within 80 min under UV light irradiation. The photocatalytic activity of $\text{CQDs}/\text{Ag}_2\text{O}$ is superior to Ag_2O (45%), $\text{Ag}/\text{Ag}_2\text{O}$ (63%) and $\text{CQDs}/\text{Ag}_2\text{O}$ (82%) within 60 min. Under visible light irradiation pure for 120 min, Ag_2O exhibit low photocatalytic activity for degradation of MB (Fig. 8b). However, the as-synthesized $\text{Ag}/\text{Ag}_2\text{O}$ and $\text{CQDs}/\text{Ag}_2\text{O}$ can efficiently promote the photocatalytic activity as compared with the individual Ag_2O . The $\text{CQDs}/\text{Ag}/\text{Ag}_2\text{O}$ materials displayed the highest photocatalytic activity, which has a 40% improvement compared to pure Ag_2O . More significantly, the MB dye can be completely degradation under visible light irradiation. The photocatalytic performance of different materials was further explore under (N)IR light irradiation, and the results are shown in Fig. 8c. The pure Ag_2O samples exhibit very low photocatalytic performance for MB which can be negligible. Surprisingly, the photocatalytic performance of the $\text{CQDs}/\text{Ag}/\text{Ag}_2\text{O}$ ternary photocatalyst possess enhanced (N)IR photocatalytic activities compared with pure Ag_2O . The MB degradation degree for $\text{CQDs}/\text{Ag}_2\text{O}$ and $\text{CQDs}/\text{Ag}/\text{Ag}_2\text{O}$ samples is 31% and 40% under 150 min near-infrared light irradiation, respectively. In contrast, $\text{Ag}/\text{Ag}_2\text{O}$ composite have poor degradation ability, the corresponding MB degradation rate is only 10% in the same conditions. This experimental result is also consistent with the above mentioned DRS tests (Fig. 4d). In addition, the simulated solar photocatalytic activity of $\text{CQDs}/\text{Ag}/\text{Ag}_2\text{O}$ is better than of $\text{CQDs}/\text{Ag}_2\text{O}$, $\text{Ag}/\text{Ag}_2\text{O}$ and individual Ag_2O as well (Fig. 8c).

The (N)IR photocatalytic activity of the as-prepared samples were further studied by the degradation of RhB. As shown in Fig. 8f, we can see that the photodegradation rate over $\text{CQDs}/\text{Ag}/\text{Ag}_2\text{O}$ reached 48% after 150 min under (N)IR light irradiation. In control experiments using Ag_2O , $\text{Ag}/\text{Ag}_2\text{O}$ and $\text{CQDs}/\text{Ag}_2\text{O}$ as photocatalysts, no or little degradation of RhB was observed. As we all know, the water itself has a very strong absorption of electromagnetic radiation in the infrared region, and it is converted into heat [44,45]. Although we have been using circulating water cooling down the reactor vessel, the temperature of reactor is still up to 76 °C. The thermal decomposition controlled trials is carried out at 76 °C in the dark. The experimental results (Fig. 8e and f) manifested that the decolorization rate of MB and RhB were 6% and 4%, respectively. These results further confirm that the (N)IR photocatalytic property of $\text{CQDs}/\text{Ag}/\text{Ag}_2\text{O}$ is attributed to the photocatalysis reaction, not near-infrared light caused photochemical reaction or temperature effect. The above experimental results demonstrate that CQDs plays an important roles for the enhanced (N)IR photocatalytic activity. Only light with wavelengths shorter than 700 nm can be used to excite Ag_2O to generate electron-hole pairs, so the up-converted PL behavior of CQDs may make $\text{CQDs}/\text{Ag}/\text{Ag}_2\text{O}$ useful in the (N)IR light region.

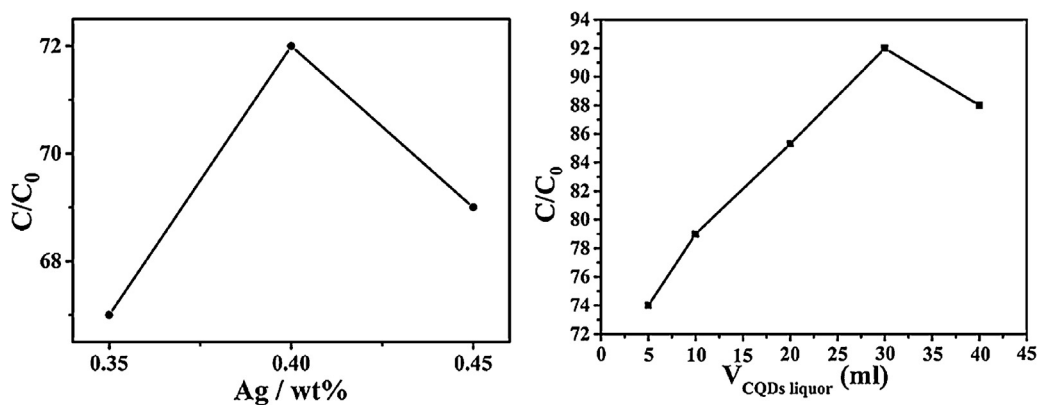


Fig. 7. Effects of Ag nanoparticles and CQDs loading amount on the photoactivity for the degradation of MB over pure Ag₂O.

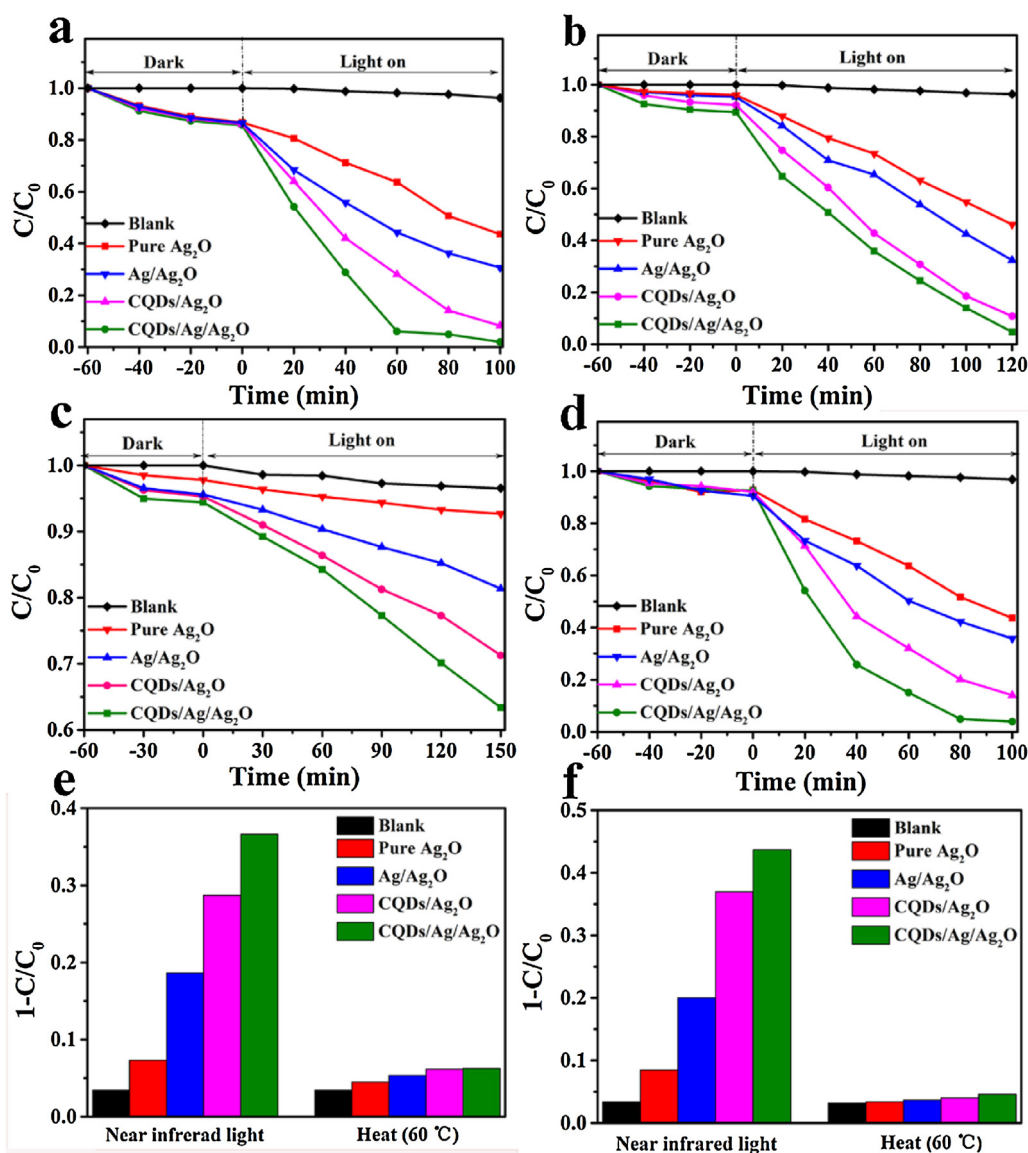


Fig. 8. photocatalytic degradation of MB in the presence of Ag₂O, Ag/Ag₂O, CQDs/Ag₂O and CQDs/Ag/Ag₂O sample under (a) UV, (b) visible, (c) (N)IR and (d) simulated sunlight irradiation; and (e, f) Photocatalytic degradation rate of MB and Rh B in the presence of Ag₂O, Ag/Ag₂O, CQDs/Ag₂O and CQDs/Ag/Ag₂O sample in the NIR light irradiation, and heat at 60 °C in the dark for 150 min.

3.3. Recycling reactions

The cycling catalytic performance of the different samples was performed five times under the same conditions (each cycle lasting

for 120 min). As shown in Fig. 9a, the photocatalytic performance of the Ag₂O is improved dramatically in second run, which may be owing to the photocorrosion led to the metallic silver formation.

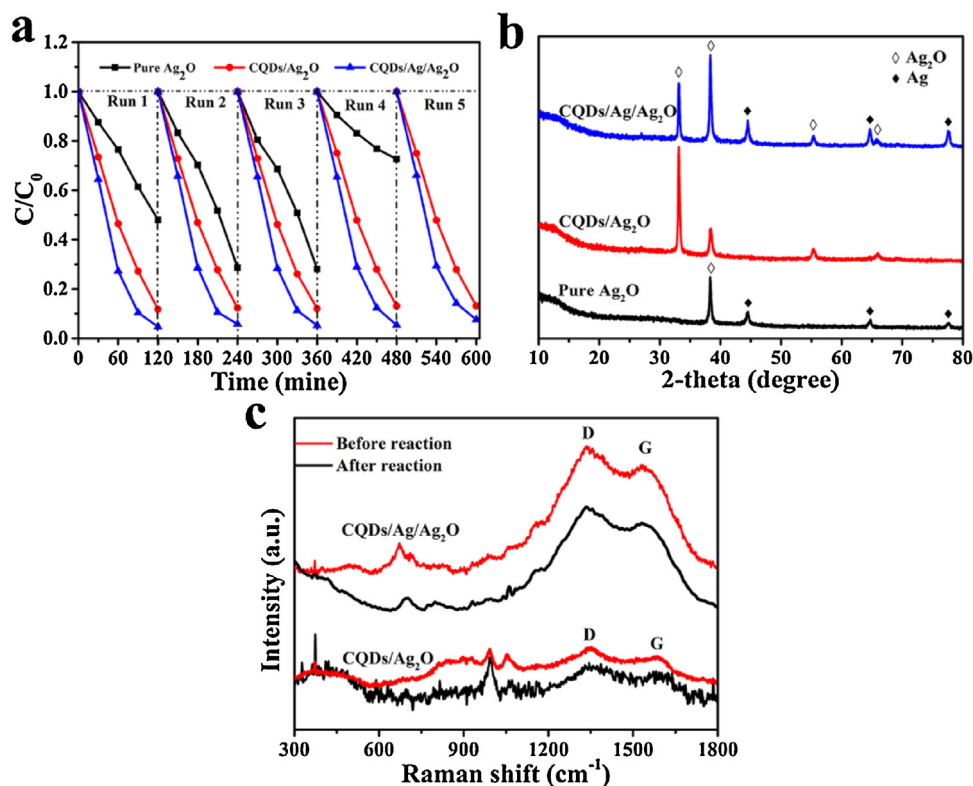


Fig. 9. (a) The repeated photocatalytic experiments for pure Ag_2O , $CQDs/Ag_2O$ and $CQDs/Ag/Ag_2O$; (b) The XRD pattern of the Ag_2O , $CQDs/Ag_2O$ and $CQDs/Ag/Ag_2O$ after 5th run cycle photocatalytic experiments; (c) Raman spectrum of $CQDs/Ag_2O$ and $CQDs/Ag/Ag_2O$ before and after 5 cycles photocatalytic experiments.

This result was demonstrated by XRD pattern of after 4th run cycle (Fig. 9b). It can be observed clearly attributable to the silver of characteristic peak. Moreover, the TEM images of pure Ag_2O after four cycles was observed (Fig. S5). It reveals that the Ag_2O surface is covered with Ag particles, which may be the main reason for the decrease of the photocatalytic activity. This phenomenon should be reasonable in terms of the competitive relation between silver content and active sites for photocatalyst degradation. Amazingly, both $CQDs/Ag_2O$ and $Ag/Ag_2O/Ag_2O$ photocatalysts have high stability and are easy to be recycled, the Raman spectra (Fig. 9c) of before and after 5th cycled reactions show no obvious differences, indicating its great promise in practical applications.

Based on all of above experimental results, two possible explanations are proposed to elaborate the significantly enhance stability of the $CQDs/Ag_2O$ and $CQDs/Ag/Ag_2O$ photocatalyst. Firstly, the coating insoluble CQDs layer over Ag_2O could effectively prevent the dissolution of the Ag_2O core in aqueous solution, thus the stability of photocatalysts can be remarkably enhanced during the photocatalytic process. More importantly, CQDs can be as electron donor and receptor, which can extract electrons from Ag_2O retards the possible photocorrosion and improves photostability of the photocatalyst significantly during the photocatalytic process [23]. As a result, CQDs may protect Ag_2O avoid photocorrosion through this electron transfer process and greatly inhibited the following transformation: $Ag_2O \rightarrow Ag + O_2$.

3.4. Possible mechanism of the photocatalytic reaction process

To evaluate the mechanism of degradation by the $CQDs/Ag/Ag_2O$ composite, the DMPO spin-trapping ESR technique and trapping experiment of active species were carried out. As shown in Fig. 10a, there are no ESR signal was observed in the dark. Under illumination, the characteristic peaks of the $DMPO \cdot O_2^-$ radicals in pure Ag_2O can be negligible. It is worth mentioning that the $\cdot O_2^-$ radicals

of $CQDs/Ag/Ag_2O$ was increased significantly, suggesting that the amount of $\cdot O_2^-$ radicals generated on the $CQDs/Ag/Ag_2O$ surface is large than that of Ag_2O . To further explore the active species on the photocatalysis process over $CQDs/Ag/Ag_2O$, the trapping experiments was executed through adding different scavengers (Fig. 10b). When the isopropyl alcohol (IPA) was added into reaction solution, the degradation rate was nearly unchanged. However, when the Vitamin C (Vc) and triethanolamine (TEOA) were added, the degradation efficiency was great inhibited. Therefore, according to the above analysis, it can be inferred that the holes and $\cdot O_2^-$ were main active species during the photocatalysis process.

On the basis of above-described experimental results, a rough energy-level diagram of the photocatalytic reaction mechanism about $CQDs/Ag/Ag_2O$ ternary photocatalyst is shown in Scheme 2. A schematic illustration is presented to explain the reasons for the degradation of organic pollution by this ternary system under full spectrum. The Ag_2O is excited by simulated solar irradiated and produces electrons and holes; the holes are consumed in photocatalytic degradation process on the Ag_2O surface [47]. Combining the fact that CQDs have a lower lowest unoccupied molecular orbital (LUMO) level than Ag_2O , when the CQDs and Ag nanoparticles were introduced simultaneously, this oxidation process is proposed the multi-steps electrons transfer instead of single step transfer for CQDs can act as both electron acceptors and donors [25–27,31,47]. On the other hand, CQDs can absorb (N)IR light, and then emit shorter wavelength light throughout the up-conversion effect, which will further excites Ag_2O to form electron-hole (e^-/h^+) pairs [30,34,47]. In view of this, the mechanism of efficient full spectra driven photoactivities degradation process was proposed: (1) when $CQDs/Ag/Ag_2O$ complex photocatalyst suspended in liquor undergo charge separation, simultaneously forming photoelectrons and holes; (2) the photogenerated electrons can be easily transferred to the CQDs layer from the conduction band (CB) of Ag_2O owing to the introduction of CQDs as an electron conductive platform, the LUMO

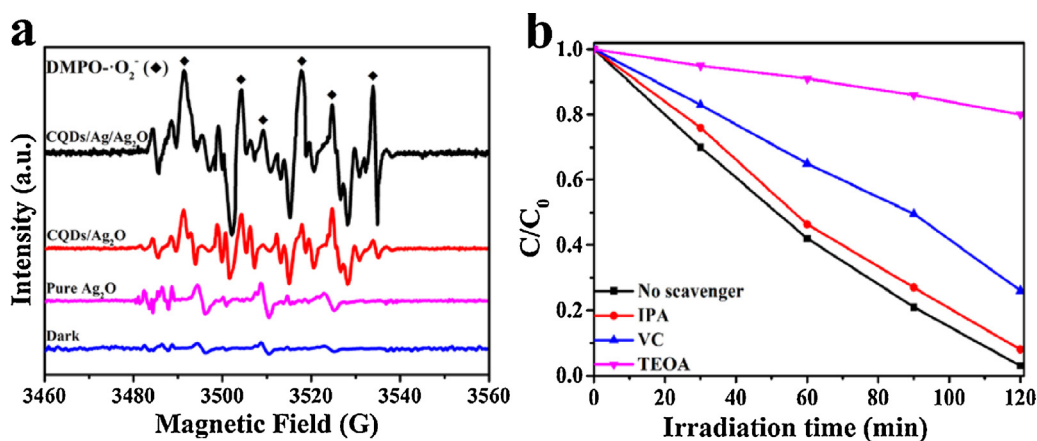


Fig. 10. (a) DMPO-ESR spin-trapping spectra of Ag₂O, CQDs/Ag₂O and CQDs/Ag/Ag₂O for detection of super oxidations ($\text{O}_2^{\bullet-}$); (b) The species trapping experiments for degradation of MB over CQDs/Ag/Ag₂O.

level of which is less than the CB of Ag₂O [25–27,31,48]; (3) the formation of Schottky junction in CQDs/Ag/Ag₂O system bring about the further transferred of photoelectrons from CQDs to Ag nanoparticles due to the SPR effect under solar light irradiation. Meanwhile, the CB edge potential of Ag₂O is located at more positive level than Fermi level of Ag nanoparticles (0.4 V vs NHE) [49–51]. Combined with the formation of the SPR effect of Schottky junction, the band structure of CQDs/Ag/Ag₂O system is shown in Scheme 2. And above all, the CQDs/Ag/Ag₂O system generates an electron-magnetic field that improve the efficiency of electron hole pair separation through the vectorial electron transfer of Ag₂O → CQDs layer → Ag. The electron-hole pairs are readily separated under the influence of the surface potential and their distance to travel to the surface of Ag₂O, where holes can be directly reacted with organic matter and electrons will be further involved in chemical reactions. Considering a more negative potential of Ag₂O, given that the redox potential of $\text{O}_2/\text{O}_2^{\bullet-}$ is -0.046 eV, the CB electrons could not reduce the O_2 . Instead, together with the photoelectrons of Ag₂O transferred to Ag, can via a one or two-electron reduction process reduce O_2 to H_2O_2 or $\text{O}_2^{\bullet-}$, respectively ($\text{O}_2 + \text{e}^- = \text{O}_2^{\bullet-}$, -0.046 V vs NHE; $\text{O}_2 + 2\text{H}^+ + 2\text{e}^- = \text{H}_2\text{O}_2$, 0.682 V vs NHE) [52,53]. The generation of H_2O_2 can be further converted $\bullet\text{OH}$ radicals by the subsequent reaction. The reactive species in the oxidation process include h^+ , $\text{O}_2^{\bullet-}$ and $\bullet\text{OH}$, theoretically. Indeed, considering the number of electrons required to capture the reaction and the process, more $\text{O}_2^{\bullet-}$ will be generated, and the species trapping experiments in accordance with the guesswork. As a result, the synergistic effect through the interfacial modified and charge-transfer channels design by use of the integration of CQDs layer and Ag play a pivot role upon the enhancement of practically photocatalytic degradation organic pollution.

4. Conclusions

In summary, highly efficient complex photocatalyst (CQDs/Ag/Ag₂O) is fabricated by combining carbon quantum dots with strong and tunable luminescence, Ag particles and silver oxide. The enhanced photocatalyst activity was mainly attributed to the synergistic effects of the following three reasons: (1) the cooperative contribution of SPR effect, efficient separation of electron-hole pairs, and prolonged lifetime of charge carries by Ag nanoparticles; (2) the cooperation of mutual-benefit of the excellent up-converted PL and electron reservoir properties of CQDs; (3) the CQDs/Ag/Ag₂O nanostructured architectures provided a favorable electron pathway, Ag₂O → CQDs → Ag, for the efficient separation of electron-hole pairs. The designed nanostructured

architectures achieved a remarkably photocatalytic activity and electron migrated capacity at full spectrum wavelengths. The findings from this study not only provided some insight into the fabrication of plasmonic photocatalysts, but also opened a new avenue for the preparation of (N)IR-sensitive photocatalyst, which can be applied to the current environmental pollution, energy and other related fields.

Acknowledgements

The authors would like to acknowledge the National Natural Science Foundation of China (No. 21546006), Natural Science Foundation of Jiangsu Province (No. BK20150536) and Six Talents Peak Project in Jiangsu Province (XNY-009).

Appendix A. Supplementary data

Supplementary data associated with this article can be found, in the online version, at <http://dx.doi.org/10.1016/j.apcatb.2016.03.056>.

References

- [1] T. Hisatomi, J. Kubota, K. Domen, *Chem. Soc. Rev.* 43 (2014) 7520–7535.
- [2] X.B. Chen, S.H. Shen, L.J. Guo, S.S. Mao, *Chem. Rev.* 110 (2010) 6503–6570.
- [3] R.S. Yuan, T. Chen, E.H. Fei, J.L. Lin, Z.X. Ding, J.L. Long, Z.Z. Zhang, X.Z. Fu, P. Liu, L. Wu, X.X. Wang, *ACS Catal.* 1 (2011) 200–206.
- [4] J.G. Hou, H.J. Chen, O. Takeda, H.M. Zhu, *Angew. Chem.* 54 (2015) 8480–8484.
- [5] S. Yu, Y.H. Kim, S.Y. Lee, H.D. Song, J. Yi, *Angew. Chem.* 53 (2014) 11203–11207.
- [6] X.B. Chen, S.S. Mao, *Chem. Rev.* 107 (2007) 2891–2959.
- [7] G. Wang, X.C. Ma, B.B. Huang, H.F. Cheng, Z.Y. Wang, J. Zhan, X.Y. Qin, X.Y. Zhang, Y. Dai, *J. Mater. Chem.* 22 (2012) 21189–21194.
- [8] J.T. Li, S.K. Cushing, P. Zheng, T. Senty, F.K. Meng, A.D. Brustow, A. Manivannan, N.Q. Wu, *J. Am. Chem. Soc.* 136 (2014) 8438–8449.
- [9] W. Zhao, J.H. Li, Z.B. Wei, S.M. Wang, H. He, C. Sun, *Appl. Catal. B: Environ.* 179 (2015) 9–20.
- [10] J.T. Li, S.K. Cushing, P. Zheng, T. Senty, F.K. Meng, A.D. Brustow, A. Manivannan, N.Q. Wu, *J. Am. Chem. Soc.* 136 (2014) 8438–8449.
- [11] S.K. Cushing, N.Q. Wu, *Interface* 22 (2013) 63–67.
- [12] S.K. Cushing, J. Li, F. Meng, T.R. Senty, S. Suri, M. Zhi, M. Li, A.D. Bristow, N.Q. Wu, *J. Am. Chem. Soc.* 134 (2012) 15033–15041.
- [13] J. Li, S. Cushing, J. Bright, F. Meng, T.R. Senty, P. Zheng, A.D. Bristow, N.Q. Wu, *ACS Catal.* 3 (2013) 47–51.
- [14] B.F. Luo, D.B. Xu, D. Li, G.L. Wu, M.M. Wu, W.D. Shi, M. Chen, *ACS Appl. Mater. Interfaces* 7 (2015) 17061–17069.
- [15] Y. Yu, C.Y. Cao, H. Liu, P. Li, F.F. Wei, Y. Jiang, W.G. Song, *J. Mater. Chem. A* 2 (2014) 1677–1681.
- [16] S.Q. Song, B. Cheng, N.S. Wu, A.Y. Meng, S.W. Cao, J.G. Yu, *Appl. Catal. B: Environ.* 181 (2016) 71–78.
- [17] G.Q. Luo, X.J. Jiang, M.J. Li, Q. Shen, L.M. Zhang, H.G. Yu, *ACS Appl. Mater. Interfaces* 5 (2013) 2161–2168.

- [18] Y. Yang, E. Liu, H. Dai, L. Kang, H. Wu, J. Fan, X. Hu, H. Liu, *Int. J. Hydrogen Energy* 39 (2014) 7664–7671.
- [19] P. Wang, B. Huang, X. Qin, X. Zhang, Y. Dai, J. Wei, M.H. Whangbo, *Angew. Chem. Int. Ed.* 47 (2008) 7931–7933.
- [20] F. Dong, Q.Y. Li, Y.J. Sun, W.K. Ho, *ACS. Catal.* 4 (2014) 4341–4350.
- [21] Q. Kang, T. Wang, P. Li, L. Liu, K. Chang, M. Li, J.H. Ye, *Angew. Chem. Int. Ed.* 54 (2015) 841–845.
- [22] Z.H. Zhang, R.B. Dua, L.B. Zhang, H.B. Zhu, H.N. Zhang, P. Wang, *ACS Nano* 7 (2013) 1709–1717.
- [23] L. Dai, D.K. Chang, J.B. Baek, W. Lu, *Small* 8 (2012) 1130–1166.
- [24] H.Z. Zhang, L.H. Guo, D.B. Wang, L.X. Zhao, B. Wan, *ACS Appl. Mater. Interfaces* 7 (2015) 1816–1823.
- [25] H.C. Zhang, H. Huang, H. Ming, H.T. Li, L.L. Zhang, Y. Liu, Z.H. Kang, *J. Mater. Chem.* 22 (2012) 10501–10506.
- [26] J. Liu, Y. Liu, N.Y. Liu, Y.Z. Han, X. Zhang, H. Huang, Y. Lifshitz, S.T. Lee, J. Zhong, Z.H. Kang, *Science* 347 (2015) 970–974.
- [27] H.T. Li, Z.H. Kang, Y. Liu, S.T. Lee, *J. Mater. Chem.* 22 (2012) 24230–24253.
- [28] X.T. Zheng, A. Ananthanarayanan, K.Q. Luo, P. Chen, *Small* 11 (2015) 1620–1636.
- [29] Y.F. Wang, A.G. Hu, *J. Mater. Chem. C* 2 (2014) 6921–6939.
- [30] J. Tian, Y.H. Leng, Z.H. Zhao, Y. Xia, Y.H. Sang, P. Hao, J. Zhan, M.C. Li, H. Liu, *Nano Energy* 11 (2015) 419–427.
- [31] X. Zhang, H. Huang, J. Liu, Y. Liu, Z. Kang, *J. Mater. Chem. A* 1 (2013) 11529–11533.
- [33] H. Huang, H.L. Hu, S. Qiao, L. Bai, M.M. Han, Y. Liu, Z.H. Kang, *Nanoscale* (2013) 1–3.
- [34] X.Y. Xia, N. Deng, G.W. Cui, J.F. Xie, X.F. Shi, Y.Q. Zhao, Q. Wang, W. Wang, B. Tang, *Chem. Commun.* 51 (2015) 10899–10902.
- [35] S.J. Zhu, Q.N. Meng, L. Wang, J.H. Zhang, Y.B. Song, H. Jin, K. Zhang, H.C. Sun, H. Wang, B. Yang, *Angew. Chem. Int. Ed.* 52 (2013) 3953–3957.
- [36] H. Huang, H.L. Hu, S. Qiao, L. Bai, M.M. Han, Y. Liu, Z.H. Kang, *Nanoscale* 52 (2013) 3953–3957.
- [37] Y.Z. Han, H. Huang, H.C. Zhang, Y. Liu, X. Han, R.H. Liu, H.T. Li, Z.H. Kang, *ACS Catal.* 4 (2014) 781–787.
- [38] J. Gao, F. Liu, Y. Liu, N. Ma, Z. Wang, X. Zhang, *Chem. Mater.* 22 (2010) 2213–2218.
- [39] Z.H. Sun, J.J. Guo, S.M. Zhu, L. Mao, J. Ma, D. Zhang, *Nanoscale* 6 (2014) 2186–2193.
- [40] Y. Ma, H. Xu, Y. Zeng, C.L. Ho, C.H. Chui, Q. Zhao, W. Huang, W.Y. Wong, *J. Mater. Chem. C* 3 (2015) 66–72.
- [41] S. Bai, J. Ge, L. Wang, M. Gong, M. Deng, Q. Kong, L. Song, J. Jiang, Q. Zhang, Y. Luo, Y. Xie, Y. Xiong, *Adv. Mater.* 26 (2014) 5689–5695.
- [42] Z.H. Zhang, R.B. Dua, L.B. Zhang, H.B. Zhu, H.N. Zhang, P. Wang, *ACS Nano* 7 (2013) 1709–1717.
- [43] S.I. In, D.D. Vaughn II, R.E. Schaak, *Angew. Chem. Int. Ed.* 51 (2012) 3915–3918.
- [44] J. Tian, Y.H. Sang, G.W. Yu, H.D. Jiang, X.N. Mu, H. Liu, *Adv. Mater.* 25 (2013) 5075–5080.
- [45] Y.H. Sang, Z.H. Zhao, M.W. Zhao, P. Hao, Y.H. Leng, H. Liu, *Adv. Mater.* 27 (2015) 363–369.
- [47] H. Zhang, L.X. Zhao, F.L. Geng, L.H. Guo, B. Wan, Y. Yang, *Appl. Catal. B: Environ.* 180 (2016) 656–662.
- [48] J. Liu, H.C. Zhang, D. Tang, X. Zhang, L.K. Yan, Y.Z. Han, H. Huang, Y. Liu, Z.H. Kang, *ChemCatChem* 6 (2014) 2634–2641.
- [49] X. Xiao, L. Ge, C. Han, Y. Li, Z. Zhao, Y. Xin, S. Fang, L. Wu, P. Qiu, *Appl. Catal. B* 163 (2015) 564–572.
- [50] H. Tada, T. Kiyonaga, S. Naya, *Chem. Soc. Rev.* 38 (2009) 1849–1858.
- [51] X. Wang, S. Li, Y. Ma, H. Yu, J. Yu, *J. Phys. Chem. C* 115 (2011) 14648–14655.
- [52] P. Wang, Y. Xia, P. Wu, X. Wang, H. Yu, J. Yu, *J. Phys. Chem. C* 118 (2014) 8891–8898.
- [53] Y.Z. Hong, Y.H. Jiang, C.S. Li, W.Q. Fan, X. Yan, M. Yan, W.D. Shi, *Appl. Catal. B: Environ.* 180 (2016) 663–673.